AD_____

Award Number: W81XWH-04-1-0697

TITLE: Alpha-v Integrin Targeted PET Imaging of Breast Cancer Angiogenesis and Low-Dose Metronomic Anti-Angiogenic Chemotherapy Efficacy

PRINCIPAL INVESTIGATOR: Xiaoyuan Chen, Ph. D.

CONTRACTING ORGANIZATION: Leland Stanford Junior University
Stanford CA 94305-4125

REPORT DATE: August 2006

TYPE OF REPORT: Annual

PREPARED FOR: U.S. Army Medical Research and Materiel Command
Fort Detrick, Maryland 21702-5012

REPORT DOCUMENTATION PAGE

Form Approved
OMB No. 0704-0188

1. REPORT DATE *(DD-MM-YYYY)*	**2. REPORT TYPE**	**3. DATES COVERED** *(From - To)*
01-08-2006	Annual	15 Jul 2005 –14 Jul 2006

4. TITLE AND SUBTITLE
Alpha-v Integrin Targeted PET Imaging of Breast Cancer Angiogenesis and Low-Dose Metronomic Anti-Angiogenic Chemotherapy Efficacy

5a. CONTRACT NUMBER

5b. GRANT NUMBER
W81XWH-04-1-0697

5c. PROGRAM ELEMENT NUMBER

6. AUTHOR(S)
Xiaoyuan Chen, Ph. D.

E-Mail: shawchen@stanford.edu

5d. PROJECT NUMBER

5e. TASK NUMBER

5f. WORK UNIT NUMBER

7. PERFORMING ORGANIZATION NAME(S) AND ADDRESS(ES)
Leland Stanford Junior University
Stanford CA 94305-4125

8. PERFORMING ORGANIZATION REPORT NUMBER

9. SPONSORING / MONITORING AGENCY NAME(S) AND ADDRESS(ES)
U.S. Army Medical Research and Materiel Command
Fort Detrick, Maryland 21702-5012

10. SPONSOR/MONITOR'S ACRONYM(S)

11. SPONSOR/MONITOR'S REPORT NUMBER(S)

12. DISTRIBUTION / AVAILABILITY STATEMENT
Approved for Public Release; Distribution Unlimited

13. SUPPLEMENTARY NOTES - Original contains colored plates: ALL DTIC reproductions will be in black and white.

14. ABSTRACT:
The overall objective of this project is to develop 18F-labeled RGD peptide derivatives for breast cancer imaging with prolonged tumor retention and improved in vivo kinetics to visualize and quantify αv-integrin expression and subsequently evaluate the metronomic anti-angiogenic chemotherapy efficacy on tumor regression, necrosis, and angiogenesis. Specific Aims: (1) To optimize 18F-labeled RGD peptide tracer for breast cancer imaging with prolonged tumor retention and improved in vivo kinetics. (2) To demonstrate the feasibility of PET/18F-RGD to image breast tumor growth, spread, and angiogenesis as well as quantifying αv-integrin expression level during breast tumor neovascularization over time. (3) To evaluate the efficacy of EMD 121974/paclitaxel combination on tumor regression, necrosis, and angiogenesis and demonstrate the feasibility of PET/18F-RGD to monitor the treatment outcomes. Major findings: We have previously reported that 18F-FB-E[c(RGDyK)]2 (18F-FRGD2) allows quantitative PET imaging of integrin αvβ3 expression. However, the potential clinical translation was hampered by the relatively low radiochemical yield. We thus developed a new tracer 8F-FB-mini-PEG-E[c(RGDyK)]2 (18F-FPRGD2) that has improved radiolabeling yield without compromising the tumor targeting efficiency and in vivo kinetics. We also showed that RGD-Pacitaxel treatment cause significant reduction in tumor growth in integrin positive MDA-MB-435 breast cancer model, which is superior to the combination of RGD and paclitaxel.

15. SUBJECT TERMS
None provided

16. SECURITY CLASSIFICATION OF:			**17. LIMITATION OF ABSTRACT**	**18. NUMBER OF PAGES**	**19a. NAME OF RESPONSIBLE PERSON**
a. REPORT	**b. ABSTRACT**	**c. THIS PAGE**			USAMRMC
U	U	U	UU	16	**19b. TELEPHONE NUMBER** *(include area code)*

Standard Form 298 (Rev. 8-98)
Prescribed by ANSI Std. Z39.18

Table of Contents

INTRODUCTION

During the first year of the funding period, we have found that dimeric RGD peptide tracer [^{18}F]FB-E[c(RGDyK)]$_2$ (abbreviated as [^{18}F]FRGD$_2$) has high integrin binding $\alpha_v\beta_3$ affinity and specificity in vitro and in vivo. However, the overall yield of ^{18}F-FRGD2 was not satisfactory, due in part, to the bulk of the two cyclic pentapeptides and the prosthetic group *N*-succinimidyl-4-^{18}F-fluorobenzoate (^{18}F-SFB). During the year 2 of the funding period, we incorporated a mini-PEG spacer, 11-amino-3,6,9-trioxaundecanoic acid, with three ethylene oxide units, onto the glutamate α-amino group of the dimeric RGD peptide E[c(RGDyK)]$_2$ (denoted as RGD2). The mini-PEG spacered dimeric RGD peptide was labeled with ^{18}F through ^{18}F-SFB and evaluated in murine tumor models by microPET imaging. Extensive in vitro, ex vivo, and in vivo experiments were carried out to evaluate the tumor targeting efficacy and pharmacokinetics of ^{18}FPRGD2, which was compared with previously reported ^{18}F-FRGD2.

During the first year of the funding period, we have also demonstrated that RGD peptide inhibits cell cycle by arresting cells in G0/G1 phase. The RGD-paclitaxel conjugate inhibited cell proliferation with an activity comparable to that observed for paclitaxel, both of which were mediated by an arrest in G2/M phase of the cell cycle followed by apoptosis. Biodistribution studies of ^{125}I-E[c(RGDyK)]$_2$ and ^{125}I- E[c(RGDyK)]$_2$-paclitaxel conjugate in integrin positive MDA-MB-435 breast cancer model also showed that the RGD-PTX conjugate is αvβ3 specific and that tumor retention is high and persistent. This indicates the effectivenss of a dimeric RGD peptide to deliver chemotherapeutic drugs such as paclitaxel to the desired tumor site. In the second year of the funding period, we have tested the treatment efficacy of the RGD-PTX conjugate in an orthotopic MDA-MB-435 breast cancer model and followed the treatment efficacy with non-invasive imaging techniques.

BODY

Part I: Development of ^{18}F-labeled mini-PEG spacered RGD dimer (^{18}F-FPRGD2)

Starting from ^{18}F-F$^-$, the total synthesis time of ^{18}F-FPRGD2 was about 180 min and the overall decay-corrected yield was over 40%. The much improved synthesis yield of ^{18}F-FPRGD2 makes it feasible for clinical translation. For example, starting from 37 GBq (1 Ci) of ^{18}F-F-, about 4-5 GBq (100-140 mCi) of ^{18}F-FPRGD2 can be synthesized in 3 h (enough for 3-5 patients).

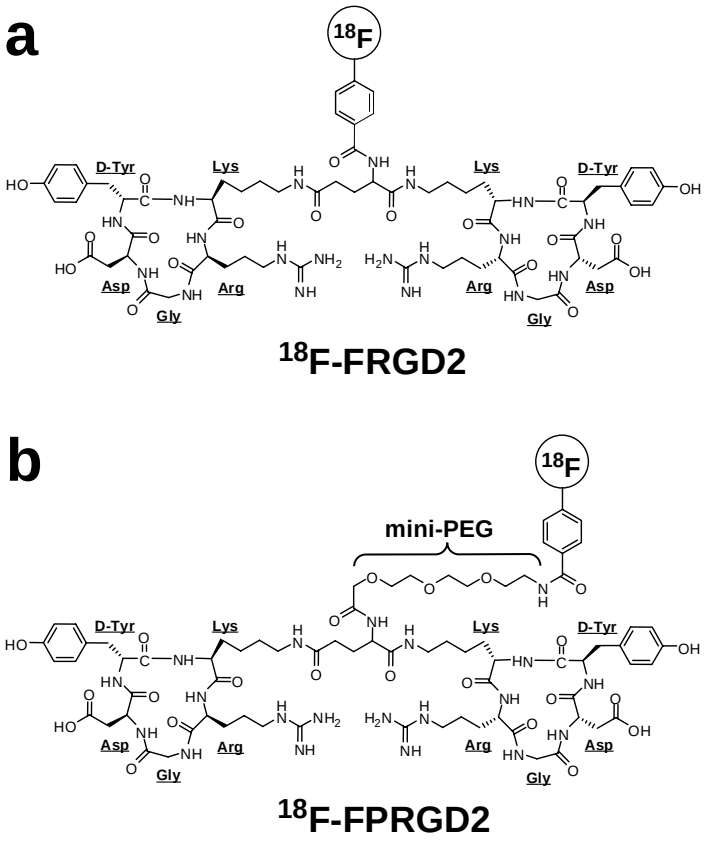

Fig. 1. Chemical structures of ^{18}F-FRGD2 (a) and ^{18}F-FPRGD2 (b). The only difference between the two structures is the mini-PEG spacer.

The octanol/water partition coefficient (logP) for ^{18}F-FPRGD2 was -2.28 ±0.05 (^{18}F-FRGD2: -2.10 ± 0.03), indicating that the tracer is slightly more hydrophilic than ^{18}F-FRGD2 after incorporation of the mini-PEG spacer.

The receptor-binding affinity of PRGD2 and FPRGD2 was evaluated using U87MG cells (integrin $\alpha_v\beta_3$-positive). Both peptides inhibited the binding of ^{125}I-echistatin (integrin $\alpha_v\beta_3$ specific) to U87MG cells in a concentration dependent manner. The IC_{50} values for PRGD2 and FPRGD2 were 70.1 ± 3.5 and 40.6 ± 4.6 nmol/L (n = 3) respectively,

comparable to that of FRGD2 (55.1 ± 6.5 nmol/L). Due to the presence of the mini-PEG linker and/or the prosthetic group (FB), all three peptides had slightly lower binding affinity than RGD2 (IC_{50} = 26.1 ± 3.2 nmol/L). The comparable IC_{50} values of FRGD2 and FPRGD2 suggest that incorporation of a mini-PEG linker had minimal effect on the receptor binding. It is of note that cell-based receptor binding assay typically give higher IC_{50} values (lower binding affinity) than those measured by ELISA or solid-phase receptor binding assay. Therefore, when comparing the receptor binding affinity (IC_{50} values), it is critical that the IC_{50} values were obtained from the same assay.

Dynamic microPET scans were performed on U87MG xenograft model and selected coronal images at different time points after injecting ^{18}F-FPRGD2 were shown in Figure 2a. High tumor uptake was observed as early as 5 min after injection. The U87MG tumor uptake was 4.9 ± 0.1, 3.4 ± 0.3, and 2.7 ± 0.1 %ID/g at 30 min, 1 h, and 2 h p.i. respectively (n = 3). Most activity in the non-targeted tissues and organs had been cleared by 1 h p.i. For example, the uptake values in the kidneys, liver, and lung were as low as 2.0 ± 0.6, 1.1 ± 0.3, and 0.5 ± 0.2 %ID/g, respectively at 1 h p.i. For direct visual comparison, representative serial microPET images of U87MG tumor mice after injection of ^{18}F-FRGD2 were also shown (Fig. 2b). It can be seen that both tracers gave comparable imaging quality, indicating that the mini-PEG spacer did not significantly alter the tumor targeting efficacy in vivo. Because of the very low tracer uptake in most organs especially in the abdominal region, ^{18}F-FPRGD2 is suitable for imaging integrin positive lesions in most areas except for the kidneys and the urinary bladder. Time-activity curves showed that this tracer excreted predominantly through the renal route.

The integrin $\alpha_v\beta_3$ specificity of ^{18}F-FPRGD2 in vivo was confirmed by a blocking experiment where the tracer was co-injected with c(RGDyK) (10 mg/kg). As can be seen from Figure 2c, the U87MG tumor uptake in the presence of non-radiolabeled RGD peptide (0.5 ± 0.2 %ID/g) is significantly lower than that without RGD blocking (3.4 ± 0.3 %ID/g) ($P < 0.001$). Similar as previously reported, the tracer cleared from the body significantly faster and the uptake in most organs (e.g. kidneys and liver) were also lower than those without c(RGDyK) blocking. Western blot and immunohistochemical staining also confirmed that these organs express low levels of integrin $\alpha_v\beta_3$ (data not shown).

The c-neu oncomice, a spontaneous tumor model which is more clinically relevant than the U87MG xenograft model, was also injected with ^{18}F-FPRGD2 and scanned in the microPET scanner (Fig. 2d). This spontaneous breast tumor has been well-established in the literature to be integrin $\alpha_v\beta_3$-positive [27-30]. The spontaneous tumor uptake at 30 min p.i. was 3.6 ± 0.1 %ID/g (n = 2), slightly higher than the kidney uptake (3.1 ± 0.5 %ID/g). The non-specific uptake in all the other organs was at background level (< 1.5 %ID/g). The tumor uptake dropped to 2.4 ± 0.1 %ID/g at 1 h p.i. Successful imaging of this spontaneous tumor model suggests the usefulness of ^{18}F-FPRGD2 in detecting integrin $\alpha_v\beta_3$-positive lesions in the clinical settings.

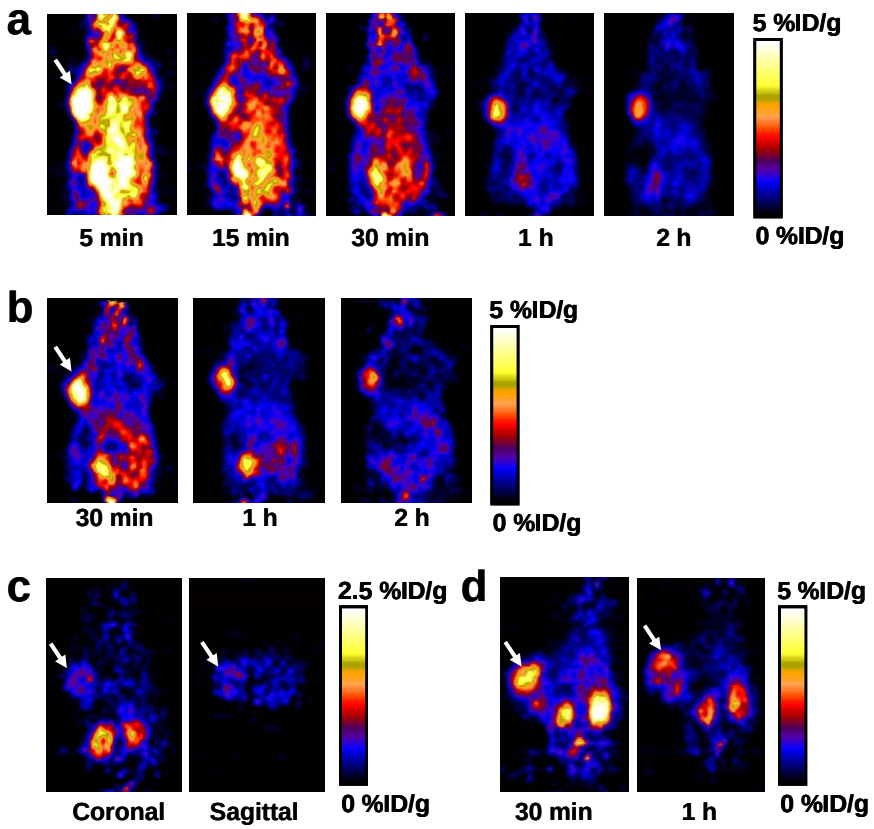

Fig. 2. (a) Serial microPET images of U87MG tumor-bearing mice after intravenous injection of ^{18}F-FPRGD2. (b) For direct visual comparison, serial microPET images of U87MG tumor-bearing mice after intravenous injection of ^{18}F-FRGD2 are also shown. (c) Coronal and sagittal microPET images of a U87MG tumor-bearing mouse 1 h after co-injection of ^{18}F-FPRGD2 and a blocking dose of c(RGDyK). Note that the scale (0-2.5 %ID/g) is different from those in (a) and (b) (0-5 %ID/g). (d) MicroPET images of a c-neu oncomouse after intravenous injection of ^{18}F-FPRGD2. Arrows indicate tumors in all cases.

Part II: In Vivo Treatment Efficacy of RGD-PTX

The *in vivo* efficacy of dimeric RGD-paclitaxel was evaluated in two independent studies using nude mice xenograft model of MDA-MB-435 cells. In the first example, RGD-paclitaxel conjugate was given at only 10 mg/kg over five days and repeated again after a week of rest and followed for extended period of time (Fig. 3). We observed significant reduction in tumor size ($p < 0.05$ at day 58), with no apparent toxicity ($n = 5$ per group). In the second experiment, animals were treated with five i.p. injections with three days intervals of saline (controls), 15 mg/kg RGD plus 10 mg/kg of paclitaxel, and 25 mg/kg of RGD-paclitaxel conjugate. The animals were monitored biweekly up to 18 days after treatment started. Fig. 4 shows the volume (mean ± SD) of drug treated MDA-MB-435 xenografts over time. A moderate but significant reduction was observed with combination treatment ($p < 0.05$ at day 18). Significant reduction in tumor growth was

observed with the conjugate ($p < 0.05$ after day 6) (n = 6 per group). Treatment with both RGD and its paclitaxel conjugate was well tolerated and did not result in drug-related deaths. Furthermore, no changes in body weight compared to vehicle control were observed with drug treatment.

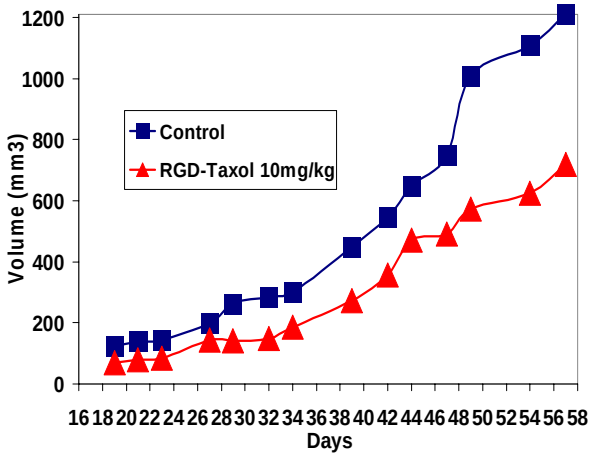

Fig. 3. Athymic nude mice (n = 5) implanted with MDA-MB-435 cells were treated with 10 mg/kg dose of RGD-paclitaxel by daily i.p. injection for five-days and repeated after a 7-days rest. Values represent the median tumor volume for each group. At day 58 we observe 50% reduction in tumor volume ($p < 0.05$).

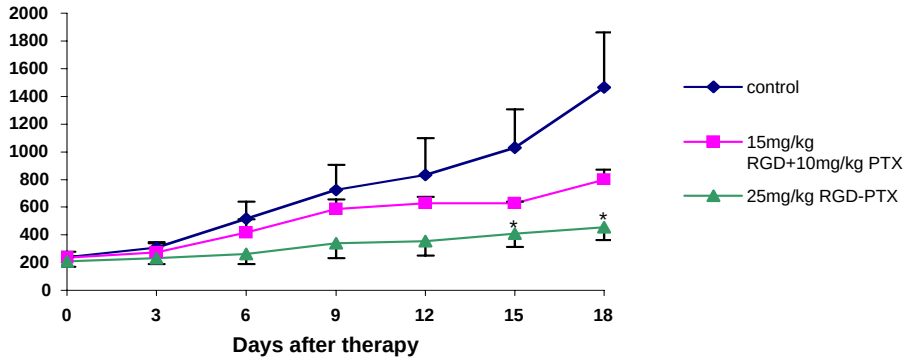

Fig. 4. Athymic nude mice (n = 10) implanted with MDA-MB-435 cells were treated with indicated doses of drugs. Values represent the median tumor volume for each group.

Representative coronal images of ^{18}F-FDG and ^{18}F-FLT (100 μCi/mouse) at 1 h after injection for MDA-MB-435 tumor mice treated with PBS, RGD/paclitaxel mixture (15 mg/kg RGD + 10 mg/kg paclitaxel), and RGD-PTX conjugate (25 mg/kg) (5 dose every three days) are shown in Fig. 5. ^{18}F-FDG PET imaging showed significant differences in tumor uptake and tumor to background signal ratio (T/B) between control and RGD-PTX conjugate treatment mice, but no significant differences between control and RGD + PTX combination treatment. ^{18}F-FLT tumor accumulation in mice was also significantly reduced after five doses of RGD-PTX conjugate, indicating decreased DNA synthesis upon treatment. The quantitative PET imaging not only showed the difference of tumor

metabolism (FDG/PET) and proliferation (FLT/PET) but also illustrated reduced tumor size after treatment.

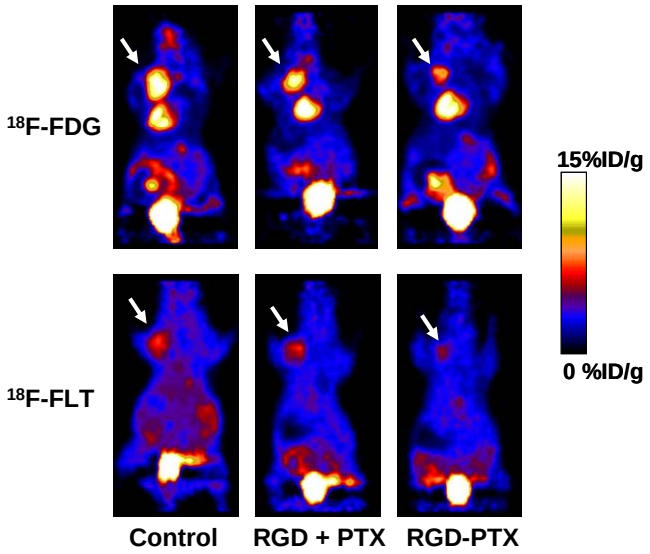

Fig. 5. ^{18}F-FDG/PET and ^{18}F-FLT/PET imaging showed that the tumor uptake follows the order of control > RGD + PTX > RGD-PTX, indicating the effectiveness of the RGD-PTX conjugate over PTX alone in terms of reducing the tumor metabolism (^{18}F-FDG/PET) and tumor proliferation (^{18}F-FLT/PET). Arrows indicate tumors in all cases.

KEY RESEARCH ACCOMPLISHMENTS

- Developed a new dimeric RGD peptide tracer [^{18}F]FPRGD2 for PET imaging of tumor integrine expression;
- Tested the treatment efficacy of dimeric RGD peptide-paclitaxel conjugate in orthotopic breast cancer model;
- In vivo treatment showed better anti-cancer effect of RGD-paclitaxel than RGD + paclitaxel combination.

REPORTABLE OUTCOMES

1. Xiong Z, Cheng Z, Zhang X, Patel M, Wu JC, Gambhir SS, Chen X.
   Imaging chemically modified adenovirus for targeting tumor expressing integrin $\alpha_v\beta_3$ in living mice with positron emission tomography.
   J Nucl Med. 2006;47:130-139 (Cover feature).

2. Zhang X, Cai W, Cao F, Schreibmann E, Wu Y, Wu JC, Xing L, Chen X.
   ^{18}F-labeled bombesin analogs for targeting GRP receptor-expressing prostate cancer.
   J Nucl Med. 2006;47:492-501.

3. Cai W, Zhang X, Wu Y, Chen X.
   A thiol-reactive ^{18}F-labeling agent, N-[2-(4-^{18}F-fluorobenzamido)ethyl]maleimide, and synthesis of RGD peptide-based tracer for PET imaging of $\alpha_v\beta_3$ integrin expression.
   J Nucl Med. 2006;47(7):1172-1180.

4. Cao F, Lin S, Krishnan M, Ray P, Patel M, Drukker M, Dylla SJ, Connolly AJ, Chen X, Weissman I, Gambhir SS, Wu JC
   In Vivo Visualization of Embryonic Stem Cell Survival, Proliferation, Migration, and Ablation after Cardiac Delivery
   Circulation. 2006;113(7):1005-14.

5. Chen X
   Multimodality Imaging of Tumor Integrin alpha(v)beta(3) Expression.
   Mini Rev Med Chem. 2006;6(2):227-34.

6. Wu Y, W Cai, Chen X.
   Near-Infrared Fluorescence Imaging of Tumor Integrin $\alpha_v\beta_3$ Expression with Cy7-Labeled RGD Multimers.
   Mol Imaging Biol. 2006;8(4):226-36.

7. Cai W, Shin D-W, Wu Y, Cao Q, Gheysens O, Gambhir SS, Wang SX, Chen X
   Peptide-labeled NIR quantum dot for cancer imaging *in vivo*
   Nano Letters. 2006;6:669-676.

8. Cai W, Chen X.
   Anti-Angiogenic Cancer Therapy Based on Integrin Antagonism
   Current Medicinal Chemistry-Anti-Cancer Agents (CMC-ACA). 2006;6:407-428.

9. Dayam R, Aiello F, Wu Y, Garofalo A, Chen X, Neamati N.
   Discovery of Small Molecule Integrin αvβ3 Receptor Antagonists as Novel Anticancer Agents
   J Med Chem. 2006;49(15):4526-34.

10. Cai W, Wu Y, Chen K, Tice DA, Chen X

In Vitro and *In Vivo* Characterization of ^{64}Cu-Labeled Abegrin™, a Humanized Monoclonal Antibody against Integrin $\alpha_v\beta_3$
Cancer Res. 2006;66(19):9673-81.

11. Hsu AR, Hou LC, Veeravagu A, Greve JM, Vogel H, Tse VCK, Chen X
In Vivo Near-Infrared Fluorescence Imaging of Integrin $\alpha_v\beta_3$ in an Orthotopic Glioblastoma Model
Mol Imaging Biol. 2006;8(6):315-23.

Abstracts:

1. Zhang X, Cai W, Wu Y, Chen X.
A Thiol-Reactive ^{18}F-Labeling Agent *N*-[2-(Aminoethyl)maleimide]-4-[^{18}F]Fluorobenzamide ([^{18}F]AMFB) and the Synthesis of RGD Peptide-Based Tracer for Positron Emission Tomography Imaging of $\alpha_v\beta_3$ Integrin Expression.
AMI International Conference, Orlando, FL, March, 2006.

2. Zhang X, Xiong Z, Wu Y, Cai W, Tseng JR, Gambhir SS, Chen X.
Quantitative PET Imaging of Tumor Integrin $\alpha_v\beta_3$ Expression with [^{18}F]FRGD2
AMI International Conference, Orlando, FL, March, 2006.

3. Cai W, Shin D-W, Wu Y, Gheysens O, Cao Q, Wang SX, Gambhir SS, Chen X.
RGD peptide-labeled NIR quantum dots for imaging tumor vasculature in living subjects
AMI International Conference, Orlando, FL, March, 2006.

4. Wu Y, Cai W, Chen X.
Cy5.5-Vitaxin for in vivo optical imaging of tumor xenografts
AMI International Conference, Orlando, FL, March, 2006.

5. Wu Y, Cai W, Zhang X, Chen K, Cao Q, Tice D, Chen X.
In Vitro and In Vivo Characterization of ^{64}Cu-Labeled Vitaxin, a Humanized Monoclonal Antibody to Integrin $\alpha_v\beta_3$
AMI International Conference, Orlando, FL, March, 2006.

6. Cai W, Chen X
In vivo tumor vasculature imaging using RGD peptide-labeled near-infrared quantum dots.
Biology & Chemistry of Peptides Gordon Research Conference, Ventura, CA, Feb, 2006

7. Cao Q, Li T, Cai W, Zhang X, Chen K, Yang Y, Xing L, Chen X
Combined Integrin siRNA Therapy and Radiotherapy of Breast Cancer
97th AACR Annual Meeting, Washington, DC, April 2006

8. Zhang X, Cai W, Wu Y, Chen X

Positron Emission Tomography Imaging of $\alpha_v\beta_3$ Integrin Expression using RGD Peptide-Based Tracer Synthesized via a Novel Thiol-Reactive ^{18}F-Labeling Agent *N*-[2-(Aminoethyl)maleimide]-4-[^{18}F]Fluorobenzamide ([^{18}F]AMFB)
53rd SNM Annual meeting, San Diego, CA, June 2006

9. Cai W, Wu Y, Cao Q, Chen K, Zhang X, Tice D, Chen X
^{64}Cu-Labeled Humanized Anti-Integrin $\alpha_v\beta_3$ Monoclonal Antibody MEDI-522 for PET Imaging of Cancer
53rd SNM Annual meeting, San Diego, CA, June 2006 (Abstract #:

10. Cai W, Chen X
Peptide-labeled quantum dots for in vivo near-infrared fluorescence imaging of tumor vasculature
232nd ACS National Meeting, San Francisco, CA, September, 2006

11. Chen X
Multimodality imaging of tumor angiogenesis
232nd ACS National Meeting, San Francisco, CA, September, 2006

CONCLUSIONS

^{18}F-FPRGD2 had high activity accumulation in $\alpha_v\beta_3$-integrin rich U87MG tumors and spontaneous mammary carcinnoma after injection. Excellent image quality, high integrin $\alpha_v\beta_3$ binding affinity/specificity, and good metabolic stability comparable to ^{18}F-FRGD2 were all maintained after incorporation of the mini-PEG spacer (11-amino-3,6,9-trioxaundecanoic acid). Most importantly, the radiolabeling yield was significantly improved and the renal uptake was significantly lowered for ^{18}F-FPRGD2 than that of ^{18}F-FRGD2, all of which makes ^{18}F-FPRGD2 suitable for clinical PET applications.

The in vitro potency of RGD-paclitaxel is similar to paclitaxel, but the tumor accumulation of RGD-paclitaxel in vivo is significantly higher than paclitaxel, resulting in improved anti-cancer effect. Development of paclitaxel conjugates with further improved tumor specific cytotoxicity is currently in progress.

REFERENCES

None.

APPENDICES

None.